VIP Surface Chemistry Very Important Paper

DOI: 10.1002/anie.201410720

Programmable Engineering of a Biosensing Interface with Tetrahedral DNA Nanostructures for Ultrasensitive DNA Detection**

Meihua Lin, Jingjing Wang, Guobao Zhou, Jianbang Wang, Na Wu, Jianxin Lu, Jimin Gao, Xiaoqing Chen, Jiye Shi, Xiaolei Zuo, and Chunhai Fan**

Abstract: *Self-assembled DNA nanostructures with precise sizes allow a programmable "soft lithography" approach to engineer the interface of electrochemical DNA sensors. By using millimeter-sized gold electrodes modified with several types of tetrahedral DNA nanostructures (TDNs) of different sizes, both the kinetics and thermodynamics of DNA hybridization were profoundly affected. Because each DNA probe is anchored on an individual TDN, its lateral spacing and interactions are finely tuned by the TDN size. By simply varying the size of the TDNs, the hybridization time was decreased and the hybridization efficiency was increased. More significantly, the detection limit for DNA detection was tuned over four orders of magnitude with differentially nanostructured electrodes, and achieved attomolar sensitivity with polymeric enzyme amplification.*

There have been increasing demands for the development of rapid and sensitive biosensors in resource-limited settings, including in small clinics and for emerging infectious diseases and biological warfare.[1] However, despite rapid progress in biosensing studies, rationally designing biosensors with desirable speed and sensitivity remains a hurdle.[1c,2] In particular, it is critically important to engineer biosensing interfaces to increase the kinetics and thermodynamics of biomolecular recognition.[1c,2a] However, the currently available approaches are largely empirical and usually rely on parameter optimization.[3] To address these problems, we developed a semiquantitative approach for the rational interfacial engineering of biosensors to improve biosensing performance.

The sensitivity of biomolecular detection is limited not only by the affinity of the biomolecules but also by the interfacial properties of the biosensor.[1c] At macroscopic interfaces, the diffusion of biomolecules from the bulk solution to the surface is nearly linear in nature, whereas mass transport is dominated by radial diffusion at micro- or nanoscopic interfaces.[1c,2a] Thus, the size reduction of biosensors usually increases the mass transport rate and improves the sensitivity. Nevertheless, the limited space available in nanosensors restricts the effective (hybridizable) number of immobilized probe molecules, which reduces the probability of collision and binding of the probe and target molecules. Indeed, theoretical studies have revealed that the detection limit of a nanosensor was unlikely to exceed one femtomolar within a practical time scale.[1c,2a] In light of these difficulties, trans-scale biosensors that incorporate nanoscale features into large-sized macroscopic surfaces are expected to solve this "size dilemma".

Intuitively, nanostructures can be incorporated into a macroscopic sensor surface by either surface etching or the deposition of metal nanoparticles.[4] However, reproducibly preparing such nanostructured surfaces with well-defined surface areas remains technically difficult.[5] Photolithography potentially provides a route to the high-resolution fabrication of nanostructures but is nevertheless hampered by its high costs and the difficulty of making 3D structures.[6] Here, we developed a conceptually new "soft lithographic" strategy to programmably and reproducibly engineer a biosensing interface using well-defined 3D DNA nanostructures. Owing to their highly specific Watson–Crick base pairing, DNA molecules can be self-assembled into DNA nanostructures of various sizes, shapes, and geometries with high predictability and precision.[4c,d,7] As an elegant example, tetrahedral DNA nanostructures (TDNs) of sub-10 nm sizes have been shown to be a rigid scaffold for the oriented anchoring of DNA probes. Here, we aimed to study the DNA surface hybridization regime (kinetics and thermodynamics) with nanometer precision and programmably tune the detection limit of DNA sensors by using macroscopic gold electrodes patterned with differently sized TDNs (Figure 1).

As the test bed for our interrogation of DNA sensors, we designed five types of TDNs with different sizes: TDN-7, TDN-13, TDN-17, TDN-26, and TDN-37, in which each edge of the TDN contains 7, 13, 17, 26 or 37 base pairs, respectively.

[*] M. Lin, J. Wang, G. B. Zhou, J. Wang, N. Wu, Dr. J. Shi, Prof. X. Zuo, Prof. C. Fan
Division of Physical Biology & Bioimaging Center
Shanghai Synchrotron Radiation Facility
CAS Key Laboratory of Interfacial Physics and Technology
Shanghai Institute of Applied Physics
Chinese Academy of Sciences, Shanghai 201800 (China)
E-mail: zuoxiaolei@sinap.ac.cn
fchh@sinap.ac.cn
J. Wang, Prof. J. Lu, Prof. J. Gao
School of Medical Lab Science and Life Science
Wenzhou Medical University, Zhejiang 325035 (China)
G. B. Zhou, Prof. X. Q. Chen
School of Chemistry and Chemical Engineering
Collaborative Innovation Center of Resource-conserving & Enviroment-friendly Society and Ecological Civilization
Central South University, Hunan 410083 (China)
Dr. J. Shi
UCB Pharma, 216 Bath Road, Slough, SL1 4EN (UK)

[**] This work was financially supported by the National Basic Research Program (973 Program grant numbers 2012CB932600 and 2013CB932803), NSFC (grant numbers 91313302, 21390414, 21422508, and 21329501), the Shanghai Pujiang Project (grant number 13PJ1410700) and the Chinese Academy of Sciences.

Supporting information for this article is available on the WWW under http://dx.doi.org/10.1002/anie.201410720.

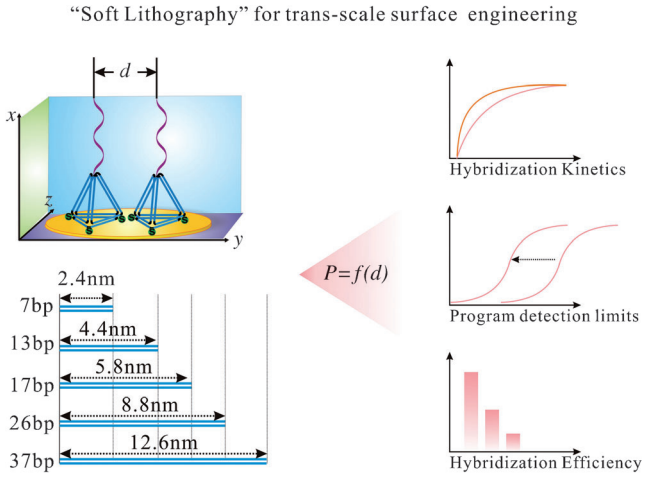

Figure 1. We developed a precisely programmable "soft lithography" method using 3D DNA tetrahedral nanostructures (TDNs) for biosensing surface engineering. Five types of TDNs with different sizes were designed (bp = base pair). The lateral distance between the DNA probes on the surface was precisely regulated through the differently sized TDNs. The surface hybridization regimes (hybridization kinetics and thermodynamics) were investigated, and the detection limits were precisely programmed.

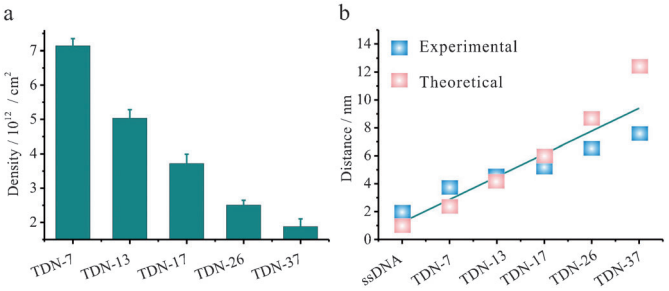

Figure 2. a) The densities of the TDNs decreased with increasing TDN size. These data were collected after the sensors reached the equilibrium. b) The interprobe distance was well controlled by tuning the size of the TDNs. The experimental data correlated highly with the theoretical data.

All TDNs were rationally designed such that no undesired secondary structures were present at the edges. Because each base pair was separated by 0.34 nm in a double helix, we were able to precisely calculate the edge length of these TDNs to be 2.4, 4.4, 5.8, 8.8, and 12.6 nm, respectively. Each TDN carries a pendant DNA probe at one vertex and three thiol groups at the other three vertices, which can be firmly anchored at the Au surface (Figure 1 and Figure S1) using well-established Au–S bonds. Native polyacrylamide gel electrophoresis (PAGE) analysis showed that these TDNs could be self-assembled, with high yields of 85–90% (Figure S2–S4). To further confirm the formation of the TDNs, we modified two strands of the TDNs (TDN-7, TDN-13, and TDN-17) with a pair of donor–acceptor dyes (Cy3 and Cy5) for fluorescence resonance energy transfer (FRET) analysis. Cy3 and Cy5 were expected to be separated by 7, 13, and 17 base pairs for TDN-7, TDN-13, and TDN-17, respectively. The presence of FRET confirmed the successful assembly of the DNA strands (Figures S2 and S3). The FRET efficiency is inversely proportional to the sixth power of the donor–acceptor distance. Consistent with this, we observed a monotonic decrease of the FRET efficiency with the increasing size of the TDNs (Figure S2). These findings indicated that the efficiency of FRET could be used as an efficient nanoscale ruler to measure the dimensions of DNA tetrahedra.

Because the lateral distance between the probes is dominated by the TDN scaffold, we were able to precisely tune the lateral distance at the nanoscale by varying the size of the TDNs. To verify this tuning effect, we first quantified the surface density of the TDN probes immobilized on a Au surface by using a cationic redox marker (hexaammineruthenium(III), Ruhex).[8] Its saturated amount of charge compensation is directly related to the number of anionic phosphate residues in the tetrahedron monolayer. We observed that the surface density of the TDN probes was inversely proportional to the size of the TDN (Figure 2a). The surface density increased from $(1.9 \pm 0.2) \times 10^{12}$ to $(7.1 \pm 0.2) \times 10^{12}$ tetrahedron per square centimeter with the decreasing size of the TDNs. We then estimated that the distances between the DNA probes were about 5.2, 4.5, and 3.7 nm for TDN-17, TDN-13, and TDN-7, respectively, which coincided well with the theoretical values (5.8, 4.4, and 2.4 nm for TDN-17, TDN-13, and TDN-7, respectively; Figure 2b). In addition, a surface density of $(3.0 \pm 0.4) \times 10^{13}$ molecules cm^{-2}, which corresponds to a distance of about 1.8 nm, was observed for a single-stranded DNA (ssDNA) probe. We also characterized the lateral distance of TDNs on the mica surface by using atomic force microscopy (AFM), which indicated that TDNs maintained their structures on the surface. Statistical analysis shows that the lateral distance is nearly linearly proportional to the TDN size (Figure S5).

With the ability to precisely regulate the distance between probes, we further investigated the surface hybridization capabilities, such as the hybridization kinetics and efficiency. The in situ hybridization investigation revealed that the kinetics of hybridization were dependent on the distance between the probes (Figure 3a and b). We observed a relatively slow hybridization process (about 90 minutes) with a distance of 1.8 nm. With an increase in distance, the hybridization kinetics improved significantly. Nearly saturated signals were observed within 10 minutes using TDN-37. To quantify the reaction rate, we calculated the pseudo-first-order reaction rate (k') using a well-established method. We discovered that the reaction rate was also distance-dependent (Figure 3b). Without using the tetrahedron, a more densely packed monolayer was formed, which reduced the reaction rate (0.01 min^{-1}). With an increase in the probe distance, the reaction rate increased monotonically. A 20-fold increase in the reaction rate (0.20 min^{-1}) was observed using TDN-37 with a probe distance of about 12.6 nm.

The hybridization efficiency also depends heavily on the distance between probes at the thermodynamic equilibrium. The hybridization efficiency was as low as 15.9% with a distance of 1.8 nm. With an increase in the distance, the hybridization efficiency initially increases and then saturates at 82% with a lateral distance of 6 nm (Figure 3c), represent-

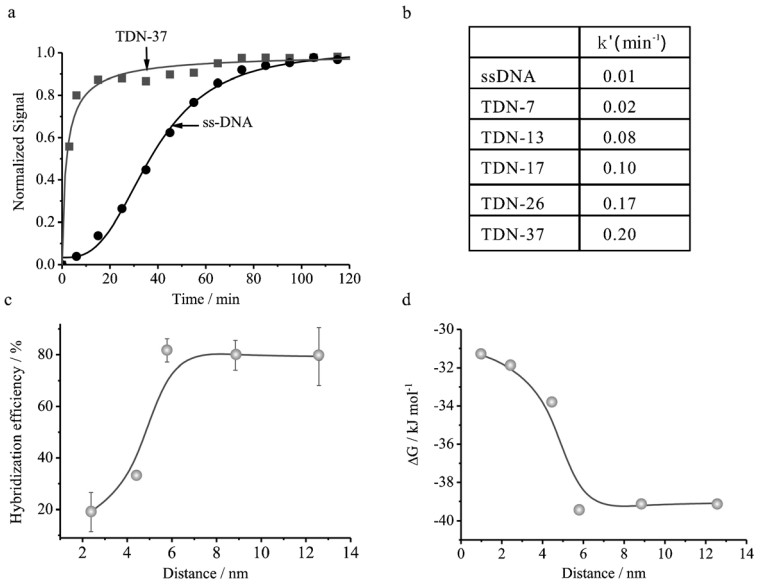

	k'(min^{-1})
ssDNA	0.01
TDN-7	0.02
TDN-13	0.08
TDN-17	0.10
TDN-26	0.17
TDN-37	0.20

Figure 3. a) Hybridization kinetics is highly related to the distance between probes. b) The pseudo-first-order reaction rates are shown. A 20-fold improvement was obtained by tuning the distance using differently sized TDNs. c) The hybridization efficiency varies with the size of TDNs. The hybridization efficiency can be improved from 15.9 to 81.5% by tuning the distance. d) The free energy of surface hybridization decreased with increasing distance between the probes, indicating that the hybridization process became more favorable.

ing a more than 5-fold increase in hybridization efficiency. Thermodynamic analysis revealed that the hybridization became more favorable when the distance between probes was increased (Figure 3d). Clearly, strong lateral interactions hinder interfacial target hybridization, whereas the reactivity and accessibility of probes for hybridization can be effectively improved by increasing the probe distance.

After understanding this distance-dependent DNA hybridization process, we further explored the biosensing capability with TDN regulation. As the test bed, we integrated the TDN probes with a well-established DNA sandwich assay. We observed that the electrochemical signal increased with the increased lateral distance. When target DNA was detected at 10 nM, an electrochemical current of about 12000 nA was obtained using TDN-26 (Figures S6 and S7). In sharp contrast, a current of only 770 nA was obtained when the distance was decreased to 1.8 nm (Figure 4 and Figures S6–S8). We then programmed the detection limits of the biosensors by regulating the distance between the probes via the use of differently sized TDNs. Interestingly, the detection limits shifted in intervals by one order of magnitude. With the increase in the TDN size, the detection limits were lowered from 10 pM (TDN-7) to 1 fM (TDN-26) (Figure 4). With this precise regulation, the detection sensitivity was improved 10000-fold. Without using the TDN scaffold, the ssDNA-based biosensor exhibited a detection limit of 10 pM by using appropriate diluent molecules (Figure S8). To further improve the sensitivity, we employed a polymerized enzyme conjugate (poly-HRP40) with 200 HRP molecules. We demonstrated that this DNA sensor reached an ultrahigh detection limit of 100 aM using TDN-26 (Figure S10). This

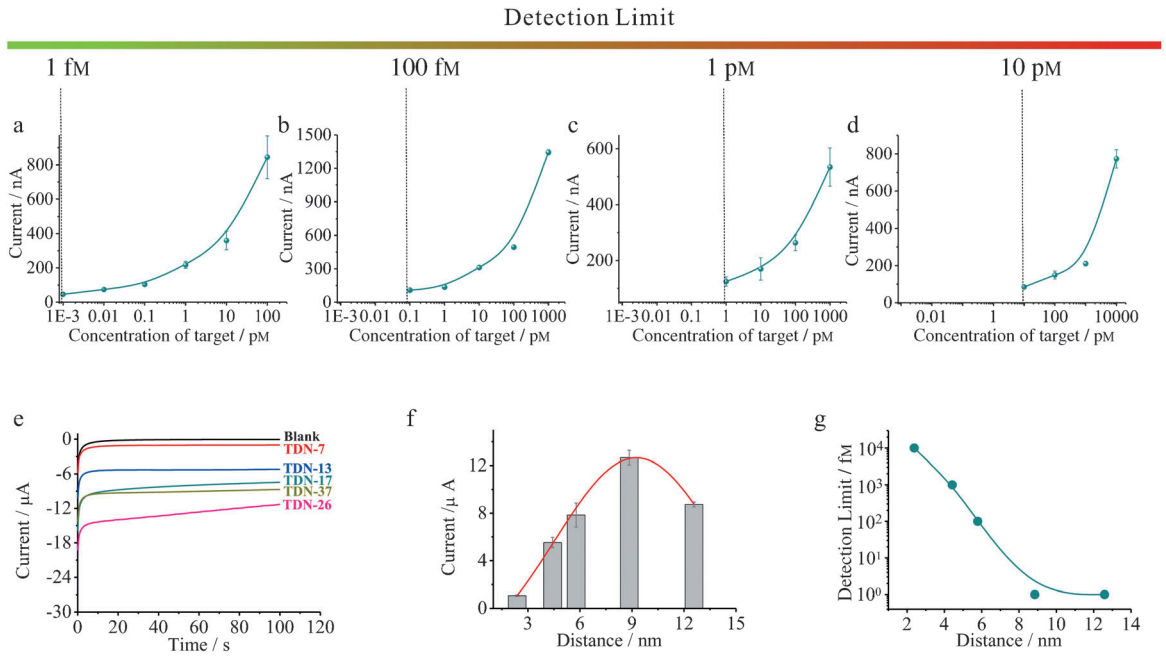

Figure 4. Detection limits can be programmed by tuning the size of the TDNs. The detection limits were 1 fM, 100 fM, 1 pM, and 10 pM for a) TDN-26, b) TDN-17, c) TDN-13, and d) TDN-7, respectively. e) Typical *I*–*t* curves for differently sized TDNs at a target concentration of 10 nM. f) The electrochemical signals vary along with lateral distance between TDNs. g) The detection limits vary along with lateral distance between TDNs.

attomolar sensitivity is comparable to the best nanostructured biosensors ever reported with sophisticated electrode fabrication and amplification.[1b,2b,9] We also note that the use of even larger TDN-37, the signal decreased as compared to TDN-26, whereas the detect limit remained nearly the same (Figure 4 f,g). This implies that the hybridization thermodynamics/kinetics are dominated by the absolute number of probes instead of mass transport as the lateral distance is beyond 8.8 nm.

The use of TDNs can improve both the probe spacing (mass transport) with significant compromise of the effective number of probes (collision possibility), which are two key factors that influence the sensitivity of a sensor. Whereas the probe densities on TDN-modified electrodes are typically lower than that on ssDNA-modified ones, the effective numbers of probes are nearly on the same order of magnitude due to the improved hybridization efficiency (Figure S9). Hence, this trans-scale TDN-based engineering provides a feasible solution to solve the "size dilemma" for sensors. In contrast, although nanoelectrodes improve the mass transport, they can only accommodate a limited number of probes. Assuming we have a nanoelectrode with a diameter of 100 nm that is modified with ssDNA probes with a density of 3.0×10^{13} molecules cm^{-2}, there are only 2355 ssDNA molecules on the nanoelectrode surface, which is about eight orders of magnitude lower than that that on our macroelectodes modified with either ssDNA or TDNs.

We then investigated the specificity and selectivity of the biosensors. The TDN-based sensors exhibited greater ability to discriminate single nucleotide mismatched targets than ssDNA-based one (Figure 5). As demonstrated, the TDN-based sensors clearly discriminated the signals from mismatched target (G) and mismatched target (A). Furthermore, the TDN-based sensors were able to selectively recognise targets in complicated matrices, such as foetal bovine serum (FBS), without an increase in background signal or a loss in signal gain (Figure 5). The signal differences in FBS and buffer solution are within 15%.

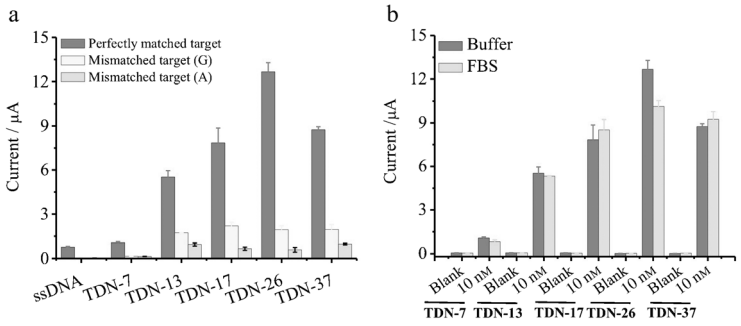

Figure 5. a) The mismatched targets exhibit relatively weak electrochemical signals, indicating that our sensors can sensitively distinguish single nucleotide polymorphisms. b) The sensors functioned well when challenged with 50% foetal bovine serum (FBS). The background signals and the signals from the 10 nM targets were comparable to those obtained in pure buffer solution.

The density, orientation and entanglement between DNA probes heavily affect their recognition process. In previous studies, a series of diluent molecules, such as mercaptohexanol (MCH), oligo(ethylene glycol)-terminated thiols and ternary small molecules, have been used as "backfillers" to help the DNA probes extend toward the solution phase.[3d,11] With these molecules, the non-specific adsorption of DNA probes on the surface can be minimized, and the orientation of the DNA probes is improved.[1c,10] However, finely tuning the density and minimizing lateral interactions remain challenging for DNA immobilization. DNA nanostructure-based soft lithography provides a feasible solution to this problem. Because the dimensions of DNA probes and the target recognition process occur on the nanometer scale, the use of DNA nanostructures offer unprecedented advantages for the bottom-up organization of DNA recognition probes with nanometer-scale precision.

To precisely control the probe density, we rationally designed TDNs with different sizes. Through these well-defined TDNs, we were able to regulate the lateral distances between the DNA probes at the nanometer scale, making it possible to investigate the DNA hybridization process with the same level of precision. Another advantage was that we could precisely anchor a single DNA probe on a single DNA nanostructure, which is very difficult to achieve with inorganic nanoparticles.[12] The third advantage was that diluent molecules were not required for immobilization, which makes the assembly of monolayers simpler by eliminating the "backfill" step.

The performance of biosensors represents a trade-off: macroscopic biosensors have a large surface area (high absolute number of probes), but their low mass transport rate and surface heterogeneity are major limitations for sensitive and rapid sensing. Nanometer-scale sensors have fast binding kinetics; however, their physical limitations in size will eventually dominate (owing to the low probability of target binding events on an individual sensor). Thus, impractically long times are required for sensitive detection using nanoscale sensors. We present a programmable "soft lithography" approach using DNA nanostructures for trans-scale surface engineering. Through this method, we bridge the gap between nanometer-scale sensors and macroscopic biosensors by combining the inherent advantages of the two approaches. Hence, our method allows the overall performance of biosensors to be improved. For example, the detection speed can be decreased from hours to minutes, and the recognition efficiency can be enhanced from 15% to greater than 80%. The detection limits can also be programmed and improved. Also importantly, the biosensors based on our trans-scale surface engineering performed well in complex matrices, revealing high applicability in real-world settings.

Experimental Section

Equimolar quantities of four strands for the formation of the tetrahedrons were mixed in buffer (20 mM Tris, 50 mM $MgCl_2$, pH 8.0) at 95°C and then cooled to 4°C.

A 3 μL volume of 1 μM tetrahedron probes in I-buffer (containing 3 mM TCEP) was added to the surface of the cleaned gold electrodes and allowed to immobilize overnight at room temperature. The immobilization for ssDNA was the same as that for the tetrahedrons, and the concentration was also 1 μM. However, for the immobilization of ssDNA, the modified electrodes were then exposed to a 2 mM MCH solution (in H-buffer) at room temperature for one hour to replace non-specific interactions and form a self-assembled monolayer (SAM) that resists non-specific adsorption of target DNA. Between each step, the electrode was rinsed with R-buffer and dried lightly with N_2 before hybridization.

DNA detection was carried out in a sandwich assay format. Different concentrations of target DNA were first mixed with the biotinylated reporter probe (100 nM) in 100 μL of H-buffer, heated to 80 °C for 5 min and then cooled under refrigeration for 5 minutes. ssDNA-probe-modified electrodes were exposed to a 2 mM MCH solution (in H-buffer) at room temperature for one hour. Finally, the tetrahedron or ssDNA-probe-modified electrode was incubated in the 100 μL solution for hybridization at 37 °C for 2 h. The electrodes were rinsed with 0.1M PBS buffer and then incubated with 3 μL of avidin-HRP (0.5 $U mL^{-1}$) for 15 minutes at room temperature. The electrodes were then extensively rinsed with R-buffer and subjected to electrochemical measurements.

Received: November 4, 2014
Published online: December 29, 2014

Keywords: biosensors · DNA nanostructures · electrochemistry · soft lithography · surface chemistry

[1] a) C. D. Chin, T. Laksanasopin, Y. K. Cheung, D. Steinmiller, V. Linder, H. Parsa, J. Wang, H. Moore, R. Rouse, G. Umviligihozo, E. Karita, L. Mwambarangwe, S. L. Braunstein, J. van de Wijgert, R. Sahabo, J. E. Justman, W. El-Sadr, S. K. Sia, *Nat. Med.* **2011**, *17*, 1015 – U1138; b) B. Lam, J. Das, R. D. Holmes, L. Live, A. Sage, E. H. Sargent, S. O. Kelley, *Nat. Commun.* **2013**, *4*, 2001; c) T. M. Squires, R. J. Messinger, S. R. Manalis, *Nat. Biotechnol.* **2008**, *26*, 417 – 426; d) Y. Xiang, Y. Lu, *Nat. Chem.* **2011**, *3*, 697 – 703; e) B. S. Ferguson, S. F. Buchsbaum, T. T. Wu, K. Hsieh, Y. Xiao, R. Sun, H. T. Soh, *J. Am. Chem. Soc.* **2011**, *133*, 9129 – 9135.

[2] a) P. E. Sheehan, L. J. Whitman, *Nano Lett.* **2005**, *5*, 803 – 807; b) L. Soleymani, Z. C. Fang, B. Lam, X. M. Bin, E. Vasilyeva, A. J. Ross, E. H. Sargent, S. O. Kelley, *ACS Nano* **2011**, *5*, 3360 – 3366.

[3] a) P. Gong, R. Levicky, *Proc. Natl. Acad. Sci. USA* **2008**, *105*, 5301 – 5306; b) A. Opdahl, D. Y. Petrovykh, H. Kimura-Suda, M. J. Tarlov, L. J. Whitman, *Proc. Natl. Acad. Sci. USA* **2007**, *104*, 9 – 14; c) A. Vallee-Belisle, F. Ricci, K. W. Plaxco, *Proc. Natl. Acad. Sci. USA* **2009**, *106*, 13802 – 13807; d) J. Wu, S. Campuzano, C. Halford, D. A. Haake, J. Wang, *Anal. Chem.* **2010**, *82*, 8830 – 8837.

[4] a) S. P. Surwade, S. C. Zhao, H. T. Liu, *J. Am. Chem. Soc.* **2011**, *133*, 11868 – 11871; b) Z. W. Li, Y. N. Gu, L. Wang, H. X. Ge, W. Wu, Q. F. Xia, C. S. Yuan, Y. Chen, B. Cui, R. S. Williams, *Nano Lett.* **2009**, *9*, 2306 – 2310; c) S. Pal, Z. T. Deng, B. Q. Ding, H. Yan, Y. Liu, *Angew. Chem. Int. Ed.* **2010**, *49*, 2700 – 2704; *Angew. Chem.* **2010**, *122*, 2760 – 2764; d) Z. Jin, W. Sun, Y. Ke, C. J. Shih, G. L. C. Paulus, Q. H. Wang, B. Mu, P. Yin, M. S. Strano, *Nat. Commun.* **2013**, *4*, 1663.

[5] J. Wirth, F. Garwe, G. Hahnel, A. Csaki, N. Jahr, O. Stranik, W. Paa, W. Fritzsche, *Nano Lett.* **2011**, *11*, 1505 – 1511.

[6] D. Qin, Y. N. Xia, G. M. Whitesides, *Nat. Protoc.* **2010**, *5*, 491 – 502.

[7] a) R. P. Goodman, I. A. T. Schaap, C. F. Tardin, C. M. Erben, R. M. Berry, C. F. Schmidt, A. J. Turberfield, *Science* **2005**, *310*, 1661 – 1665; b) S. P. Surwade, F. Zhou, B. Wei, W. Sun, A. Powell, C. O'Donnell, P. Yin, H. T. Liu, *J. Am. Chem. Soc.* **2013**, *135*, 6778 – 6781; c) J. L. Fu, M. H. Liu, Y. Liu, N. W. Woodbury, H. Yan, *J. Am. Chem. Soc.* **2012**, *134*, 5516 – 5519; d) J. P. Zheng, J. J. Birktoft, Y. Chen, T. Wang, R. J. Sha, P. E. Constantinou, S. L. Ginell, C. D. Mao, N. C. Seeman, *Nature* **2009**, *461*, 74 – 77; e) D. R. Han, S. Pal, J. Nangreave, Z. T. Deng, Y. Liu, H. Yan, *Science* **2011**, *332*, 342 – 346; f) H. Pei, N. Lu, Y. L. Wen, S. P. Song, Y. Liu, H. Yan, C. H. Fan, *Adv. Mater.* **2010**, *22*, 4754 – 4758; g) O. I. Wilner, Y. Weizmann, R. Gill, O. Lioubashevski, R. Freeman, I. Willner, *Nat. Nanotechnol.* **2009**, *4*, 249 – 254.

[8] A. B. Steel, T. M. Herne, M. J. Tarlov, *Anal. Chem.* **1998**, *70*, 4670 – 4677.

[9] a) L. Soleymani, Z. C. Fang, E. H. Sargent, S. O. Kelley, *Nat. Nanotechnol.* **2009**, *4*, 844 – 848; b) J. Hahm, C. M. Lieber, *Nano Lett.* **2004**, *4*, 51 – 54.

[10] a) H. Pei, F. Li, Y. Wan, M. Wei, H. J. Liu, Y. Su, N. Chen, Q. Huang, C. H. Fan, *J. Am. Chem. Soc.* **2012**, *134*, 11876 – 11879; b) X. M. Bin, E. H. Sargent, S. O. Kelley, *Anal. Chem.* **2010**, *82*, 5928 – 5931; c) T. Pauloehrl, A. Welle, M. Bruns, K. Linkert, H. G. Borner, M. Bastmeyer, G. Delaittre, C. Barner-Kowollik, *Angew. Chem. Int. Ed.* **2013**, *52*, 9714 – 9718; *Angew. Chem.* **2013**, *125*, 9896 – 9900; d) G. R. Abel, E. A. Josephs, N. Luong, T. Ye, *J. Am. Chem. Soc.* **2013**, *135*, 6399 – 6402; e) Y. Wen, H. Pei, Y. Shen, J. Xi, M. Lin, N. Lu, X. Shen, J. Li, C. Fan, *Sci. Rep.* **2012**, *2*, 867.

[11] a) R. J. Lao, S. P. Song, H. P. Wu, L. H. Wang, Z. Z. Zhang, L. He, C. Fan, *Anal. Chem.* **2005**, *77*, 6475 – 6480; b) C. Fan, K. W. Plaxco, A. J. Heeger, *Proc. Natl. Acad. Sci. USA* **2003**, *100*, 9134 – 9137.

[12] a) D. Zanchet, C. M. Micheel, W. J. Parak, D. Gerion, A. P. Alivisatos, *Nano Lett.* **2001**, *1*, 32 – 35; b) S. D. Jhaveri, E. E. Foos, D. A. Lowy, E. L. Chang, A. W. Snow, M. G. Ancona, *Nano Lett.* **2004**, *4*, 737 – 740.

